Reviewer 1

This is a very nice paper that should be published. I have minor suggestions.
This work reposts on results of experiments where production rates of the OH radical (R(OH)) are measured in cloud water samples. Air mass source regions for the cloud water samples are identified. Major chemical species thought to contribute to R(OH) are also measured and used in a model to calculate R(OH). These results are then compared to the measurements. Additionally, the authors use the same experimental setup employed to measure cloud water R(OH) to measure OH production in samples of single components (i.e., NO$^-$, NO_2^- and H_2O_2) in pure water. The results from these synthetic experiments are then used in the model and compared to the measured production rates.
The measurements being made are complex and tricky and it appears the authors have done the experiments with great care. The data analyses are thorough. The data quality seems reasonable; the results are in general agreement with other studies, but there is limited data to assess the quality of these experiments.

We would like to thank the reviewer for her/his interest in our work and the valuable remarks. In the revised manuscript all the corrections are indicated in blue.

1. The data interpretation is somewhat confusing and the logic of the Discussion section was somewhat unclear. I had to read through it a few times to understand the analyses approach. I suggest an attempt should be made to clarify this section. I also don’t really see the logic of it; which I would summarize as follows: -measure R(HO) in real cloud water samples. -compare to model that was run using measured NO_2^-, NO_3^-, H_2O_2, and Fe -based on the finding that the discrepancy between model and observations is highest for cloud samples with highest Fe, the authors conclude the large range in discrepancy is due to the model over-predicting R(HO) from Fe. The reason? The model does not correctly simulate Fe-organic complexes (only considers oxalate, but much more Fe is likely complexed with unidentified organic species, whereas Ferrozine analytical method includes all Fe-org complexes in the measurement of Fe, which is used in the model). -rerun the model with no Fe contribution at all to predict R(HO) - find model R(OH) is too low. - rerun the model with new synthetic (single species) photolysis rate measurements for NO_2^-, NO_3^-, H_2O_2, but still without Fe contributions.

Reply
In a first step we compared experimental and modelled R_fHO founding discrepancies. In order to better simulate and assess individually the contribution of the main photochemical sources to the generation of HO, new photolysis rates for nitrite, nitrate and hydrogen peroxide were determined experimentally. Originally, the photolysis rates for these compounds are calculated by the model using experimental quantum yields, absorption cross-sections extracted from the literature and the experimental actinic flux of the lamp. The calculated value is then subject to uncertainties and can present some differences to what is observed in the aqueous photochemical reactor. The experimental values were implemented in the M2C2 model instead of the original calculated ones. This lead to better agreement between simulated and modelled R_fHO.
Nevertheless higher differences estimated calculating the bias error (($R_{HO^\bullet}^{f}$ mod - $R_{HO^\bullet}^{f}$ exp) / $R_{HO^\bullet}^{f}$ exp in (%)) were found in samples with iron concentrations > 0.1 µM where the median of

the bias error was > 61%. In fact, the model considers only iron species under aqua-complexes or iro-oxalate complexes (in the case of Fe(III)). In the case of aqua-complexes, their photolysis represents a strong sources of hydroxyl radical. Nevertheless iron is expected to be complexed by organic compounds in cloud waters that are still not characterized. In order to support this hypothesis iron photoreactivity was considered as negligible (as expected for iron complexes) and a good agreement between experimental and modelled results was found.

2. Conclude better agreement between model – measured R(OH) suggests that model over-predicts Fe contribution and most important species is H_2O_2.
The last two steps in the sequence are interesting, but the logic is not clear to me.
Why, for example, do the authors believe their photolysis rates, which were based on overly simple experiments, versus what was originally in the model (is there a reason)?

Reply
The M2C2 model calculates the photolysis rates using experimental quantum yields, absorption cross-sections extracted from the literature and the experimental actinic flux of the lamp. These data considered in the model are subject to uncertainties. The experimental J values correspondto the effective photodegradation of H_2O_2, NO_2^- and NO_3^- in the reactor; therefore, we think that the experimental photolysis rates better represent the experimental conditions than the calculations by the model. However, the photolysis rates calculated by the model are realistic since they are in the same range of order (model : 1.52×10^{-6} s^{-1} vs. experiment: 2.5×10^{-6} s^{-1} for the H_2O_2 photolysis rates for example).

3. There is no discussion why such a simple experiment should be representative of what occurs in a chemically-complex cloud drop.

Reply
The main objective of the experimental photolysis rates calculations is to assess the contribution of each photochemical source to the hydroxyl radical formation. The next step is to consider these experimental values in the M2C2 model that considers explicit aqueous phase chemistry (see table SM1) to simulate cloud water chemistry.

3. Another analyses could be to assume the original model photolysis rates are correct for NO_2^-, NO_3^-, H_2O_2 and adjust the free Fe levels (i.e., the fraction of ferrozine-determined Fe(II)+Fe(III) that is not complexed) to achieve good agreement between modeled and measured R(OH). Data on both oxalate and TOC is available and could be included in this type of analysis.

Reply
Ferrozine method allows us to determine all Fe(II) and Fe(III) considered as free, aquacomplexes and complexed with other organic compounds. To assess the impact of iron complexation on hydroxyl radical rates, new simulations are performed. In the model, we consider 0%, 25%, 50%, 75% and 100% of the initial concentrations of iron. Part of the iron is therefore free or complexed by oxalate. The simulations are performed with the original model photolysis rates.

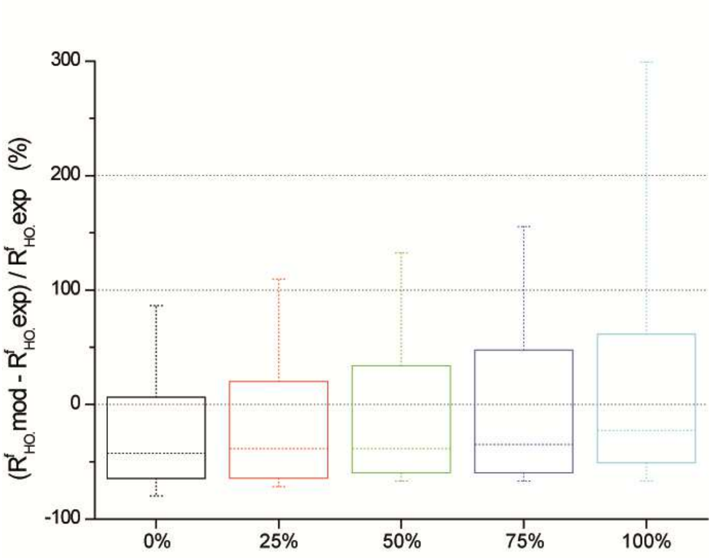

Figure 1: Distribution of the bias error for the whole cloud water samples for the reference case (100%) and considering different level of iron amounts (from 75% to 0%). The bias error is defined by the ratio ($R^f_{HO\bullet}$ *mod -* $R^f_{HO\bullet}$ *exp) /* $R^f_{HO\bullet}$ *exp in (%). The bottom and top lines correspond to the 25th and 75th percentiles, respectively. The full line represents the median values. The ends of the whiskers are the 10th and 90th percentiles.*

As shown on Figure 1, decreasing the iron amount from 100% to 0% leads to an underestimation by the model of hydroxyl radical formation rates in comparison with experimental data (median of the bias error from 22% to 42%, respectively for the iron amount equal to 100% and 0%). The figure suggests that iron photoreactivity cannot be considered as the main sources driving the hydroxyl formation rates in our cloud water samples. For this reason, the adopted approach was to modify the photolysis rates in the model that present uncertainties in their calculations. Moreover, with this new approach, the strong overestimation by the model of the hydroxyl formation rates due to the iron photolysis is neglected. The main uncertainties in the hydroxyl radical formation are related to the iron photoreactivity that strongly depends on its complexation. In fact, actually, only iron-oxalate complexes are considered in cloud chemistry models (Weller et al., 2014). Considering the around 90% of the organic matter in real cloud samples are unknown, the presence of other organic complexes is expected with various photochemical stability. However, it is quiet difficult to correlate the iron photoreactivity with the TOC due to the lack of the characterization of the organic matter.

Weller, C., Tilgner, A., Brauer, P., and Herrmann, H.: Modeling the impact of iron-carboxylate photochemistry on radical budget and carboxylate degradation in cloud droplets and particles, Environ. Sci. Technol., 48, 5652-5659, 10.1021/es4056643, 2014.

Reviewer 2

Overall comments:
Bianco et al. collected cloud waters (mostly marine origin) at a relatively high mountain site and studied their chemical compositions and photochemical formation of hydroxyl radical (OH). The measurements of chemical species were done within 24 hours after collection of those samples, which is pretty impressive. A fair number of samples were also studied to discuss the OH formation and their sources. The reviewer believes that the results presented in the manuscript, such as OH formation rates, OH sources, contribution of different OH sources and Fe(II) measurements are interesting and add valuable information to the atmospheric chemistry community. However, the reviewer also found several mistakes and mis-interpretation of the results in the manuscript.
Thus, the reviewer recommends publication of this manuscript in Atmos. Chem. Phys. after the comments as listed below are incorporated in the revised manuscript. Detailed comment:

We would like to thank the reviewer for her/his interest in our work and the valuable remarks. In the revised manuscript all the corrections are indicated in blue.

1. Pg. 13932, equation (1), RtHO = Y*RtTAOH is not right. It should be RtTAOH = Y*RtHO, since Y is the reaction yield between OH and TA, forming a fluorescent TAOH, and has a value between 0.15-0.25. To obtain RtHO, RtTAOH should be divided by Y, namely RtHO = RtTAOH /Y.

Reply
The wrong equation form has been corrected. For RfOH calculations we used the right form.

2. Pg. 13932, equation (2) should be [OH]ss = (RtTAOH)/{kOH, TA*[TA]*Y}. Actually, calculation of [OH]ss by this equation is fundamentally a mistake. This [OH]ss is for the conditions with added TA (2 mM), not for the cloud water samples by themselves. Since OH formation rates are different among cloud water samples, [OH]ss appears to show some variation, but the major sink for the OH is always TA for all the samples. Thus, OH scavenging rate constant for the experimental condition is always kOH, TA*[TA] = 4.0*109*2*10-3 = 8*106 s-1. It is not possible to calculate [OH]ss from a single OH formation rate study when high concentration of TA or any probe is added to the samples. So, please re-consider the discussion on [OH]ss.

Reply
Concerning equation (2) we have corrected our mistake reporting now the right equation.
We agree with reviewer's comment concerning the [HO]ss calculations. In the presence of an excess of TA all photogenerated hydroxyl radicals are expected to react with TA (and not with other naturally occurring scavengers). Under such conditions the HO steady-state concentration values should be different from the values expected in cloud water due to the higher value of $k_{HO^{\bullet},TA}[TA]$ compared to the value found considering the reactivity of hydroxyl radical with naturally occurring scavengers present in cloud waters (indicated as CWS_i) $k_{HO^{\bullet},CWS_i}[CWS_i]$. The

main goal of such measurement was to compare obtained values with those found in rain and cloud waters (see Table 3). Finally [HO]ss should be determined as $R^f_{HO}/k_{HO,CWSi}$*[CWSi]. The use of different TA concentration would be needed in order to determine the concentration of [HO]ss in samples considering the value at [TA]→0 following the kinetic approach reported by Anastasion and McGregor (2001).
For these reasons the data concerning the steady-state concentration of HO and related discussion were erased.

3. Pg.13929Line 19-20, in acidic solution (HCl 37%). Does it have to be very acidic? I wonder what the pH was.

Reply
HCl solution was used to obtain an acid pH as required for the nitrite detection method as reported by Kieber and Seaton. The reaction between ferrozine and nitrite was performed in acidic conditions.

4. Pg. 13929, Line28, (free or complexed). The sentence was not somehow clear to me. Do authors suggest Fe(II) is free but Fe(III) is complexed? I would guess both Fe(II) and Fe(III) can have complexed species, not just Fe2+. I appreciate clarification of the sentence.

Reply
Detection method is based on the formation of a stable and strong absorbing complex between Fe(II) and ferrozine. Considering an excess of ferrozine in solution, we can argue that all free and complexed iron can be detected using this method. In other words, the adopted method allows us to determine all Fe(II) and Fe(III) considered as free, aquacomplexes and complexed with other organic compounds.
In order to clarify this point a new sentence was added in section 2.3.

A better understanding of hydroxyl radical photochemical sources in cloud waters collected at the puy de Dôme station : Experimental *versus* modeled formation rates

A. Bianco[a,b,†], M. Passananti[a,b,†], H. Perroux[c,d], G. Voyard[a,b], C. Mouchel-Vallon[c,d], N. Chaumerliac[c,d], G. Mailhot[a,b], L. Deguillaume[c,d,*], M. Brigante[a,b,*]

[a] *Université Clermont Auvergne, Université Blaise Pascal, Institut de Chimie de Clermont-Ferrand, BP 10448, F-63000 CLERMONT-FERRAND, FRANCE*
[b] *CNRS, UMR 6296, ICCF, F-63171 AUBIERE, FRANCE*
[c] *Université Clermont Auvergne, Université Blaise Pascal, Laboratoire de Météorologie Physique, BP 10448, F-63000 CLERMONT-FERRAND, FRANCE*
[d] *CNRS, UMR 6016, LaMP, F-63171 AUBIERE, FRANCE*

* Corresponding author e-mail:
marcello.brigante@univ-bpclermont.fr
L.Deguillaume@opgc.univ-bpclermont.fr
[†] These two authors contributed equally to this work

Abstract. The oxidative capacity of the cloud aqueous phase is investigated during three field campaigns from 2013 to 2014 at the top of the puy de Dôme station (PUY) in France. Forty-one cloud samples are collected, and the corresponding air masses are classified as highly marine, marine and continental. Hydroxyl radical ($HO^{\bullet}$) formation rates ($R^{f}_{HO^{\bullet}}$) are determined using a photochemical setup (Xenon lamp that can reproduce the solar spectrum) and a chemical probe coupled with spectroscopic analysis that can trap all of the generated radicals for each sample. Using this method, the obtained values correspond to the total formation of $HO^{\bullet}$ without its chemical sinks. These formation rates are correlated with the concentrations of the naturally occurring sources of $HO^{\bullet}$, including hydrogen peroxide, nitrite, nitrate and iron. The total hydroxyl radical formation rates are measured as ranging from approximately 2×10^{-11} to 4×10^{-10} M s^{-1}, and the hydroxyl radical quantum yield formation ($\Phi_{HO^{\bullet}}$) is estimated between 10^{-4} and 10^{-2}. Experimental values are compared with modeled formation rates calculated by the model of multiphase cloud chemistry

(M2C2), considering only the chemical sources of the hydroxyl radicals. The comparison between the experimental and the modeled results suggests that the photoreactivity of the iron species as a source of $HO^\bullet$ is overestimated by the model, and H_2O_2 photolysis represents the most important source of this radical (between 70 and 99%) for the cloud water sampled at the PUY station (primarily marine and continental).

Keywords

cloud water, photochemistry, hydroxyl radical, *in situ* measurements, cloud chemistry model

1 Introduction

In the atmosphere, many trace gases are transformed by the hydroxyl radical ($HO^\bullet$), which is considered the most efficient environmental oxidant (*e.g.,* Seinfeld and Pandis, 2006). Evaluating the production of this short-lived species is crucial because it determines the fate of many chemical compounds. In atmospheric water drops and aqueous particles, the hydroxyl radical also controls the fate of inorganic and organic species (Herrmann et al., 2010). The $HO^\bullet$ - mediated oxidation of organic compounds in the aqueous phase can lead to the formation of shorter but often multifunctional organic species and, ultimately, to complete mineralization (Charbouillot et al., 2012). Complex chemical reactions catalyzed by $HO^\bullet$ can also occur in the aqueous phase forming accretion products such as oligomers (Altieri et al., 2008; Carlton et al., 2007; Perri et al., 2009; Tan et al., 2011; Ervens and Volkamer, 2010; De Haan et al., 2009). These alternative chemical pathways are efficient processes to convert organic compounds into Secondary Organic Aerosols (SOAs) (Ervens et al., 2011).

The sources of hydroxyl radicals in the aqueous phase strongly differ from those in the gas phase because of the presence of ionic species and metal ions. Aqueous phase reactants that produce $HO^\bullet$ present high concentrations in water drops and aqueous particles, likely enhancing the $HO^\bullet$ photochemical production in the condensed phase. This radical can be generated in the aqueous phase by direct photolysis of hydrogen peroxide (H_2O_2) (Herrmann et al., 2010; Yu and Barker, 2003), iron complexes (Deguillaume et al., 2005), nitrate (NO_3^-) (Zellner et al., 1990) and nitrite ions (NO_2^-) (Zafiriou and Bonneau, 1987). The other significant source of $HO^\bullet$ in cloud water is the uptake from the gas phase (Arakaki and Faust, 1998). The relative importance of the different hydroxyl radical sources depends on the chemical composition of the aqueous phase, which is also strongly variable (Deguillaume et al., 2014). $HO^\bullet$ is further scavenged in the aqueous phase, primarily by dissolved organic compounds. Evaluation of this sink is difficult because the dissolved organic matter is diverse, complex and poorly characterized (Herckes et al., 2013).

Uncertainties in $HO^\bullet$ sinks and sources make its concentrations in atmospheric water highly difficult to estimate. For this estimation, models describing the multiphase cloud chemistry have been developed and have considered the reactivity in the gas and aqueous phases along with the mass transfer between the two phases (Ervens et al., 2014; Long et al., 2013; Tilgner and Herrmann, 2010). These numerical tools allow the estimation of the steady-state concentration of $HO^\bullet$ ($[HO^\bullet]_{ss}$), which is a crucial quantity to understand the fate of atmospheric pollutants (Arakaki et al., 2013). The range of the maximal $HO^\bullet$ concentration varies from 10^{-16} to 10^{-12} M, depending on the "chemical scenario" (*i.e.,* emission/deposition and the initial chemical conditions) used in the modeling study. The amounts of organic matter and iron are key parameters controlling the $[HO^\bullet]_{ss}$. These models are expected to underestimate the radical sinks because organic scavengers cannot be exhaustively described in the aqueous chemical mechanism (Arakaki et al., 2013).

In this study, we propose the investigation of the hydroxyl radical formation in real cloud water sampled at the puy de Dôme mountain (France). The hydroxyl radical formation rate is quantified for 36 cloud water samples collected during 3 field campaigns (2013-2014). Because the main photochemical sources (hydrogen peroxide, iron, nitrite and nitrate) are also quantified, we can calculate their relative contributions to the production of the hydroxyl radicals. For this purpose, the contribution to the hydroxyl radical formation rate of more concentrated inorganic photochemical sources is investigated separately in synthetic solution. In parallel, the model of multiphase cloud chemistry (M2C2) is used to simulate $HO^\bullet$ formation rates. This model considers explicit aqueous chemical mechanisms, and a "simplified" version of the model is used to reproduce the bulk water irradiation experiments (lamp spectrum) under variable physico-chemical conditions (pH, initial concentrations of $HO^\bullet$ sources) corresponding to the cloud water samples. The comparison between the modeled and experimental $HO^\bullet$ production rates facilitates quantification of the various $HO^\bullet$ sources and enables validation of the model to reproduce the oxidative capacity of the atmospheric aqueous phase.

2 Materials and Methods

2.1 Chemicals

Hydrogen peroxide (30% in water, not stabilized), sodium nitrate (purity >99%) and ferrozine (purity >97%) were obtained from Fluka, while sodium nitrite (purity >98%) and terephthalic disodium salt (purity >99%) were purchased from ProLabo and Alfa Aesar, respectively. All of the other chemicals (purity reagent grade) used for the analysis were obtained from Sigma-Aldrich.

Solutions are prepared with deionized ultra-pure aerated milli-Q water from Millipore (resistivity = 18.2 MΩ cm) under a laminar flux hood. Moreover, glass containers and injection material are washed three times with ultra-pure water before use. If necessary, the pH values are adjusted with perchloric acid (1 N) and NaOH (1 N) using a JENWAY 3310 pH-meter within ± 0.01 pH unit. All of the solutions are stored under dark conditions, and the final preparations are performed in a room equipped with a sodium lamp (589 nm emission).

2.2 Cloud water sampling

Cloud water is sampled at the puy de Dôme (PUY) station (48°N, 2°E; 1465 m a.s.l.) in the Massif Central region (France). Three campaigns occurred during autumn 2013 from October 14th to November 6th, during spring and autumn 2014 from March 22nd to April 5th and from November 4th to 19th. During these periods, the station was primarily located in the free troposphere; thus, the air masses from various origins were not influenced by the local pollution (Hervo, 2013).

The cloud droplet sampling is performed by a one stage cloud droplet impactor (Deguillaume et al., 2014). With the air flux used, the lower limit of the aerodynamic diameter is approximately 7 µm (Brantner et al., 1994). The impactor used for this study is constructed of stainless steel and aluminum, and cloud droplets are collected by impaction onto a rectangular aluminum plate with an average sampling time of two hours. Cloud water samples are filtered using a 0.45 µm PTFE filter within 10 minutes after sampling to eliminate all of the microorganisms and particles that can interfere with the spectroscopic analysis.

Measurements performed immediately after cloud collection are conductivity, redox potential, pH, UV-visible spectroscopy, H_2O_2 and iron concentrations. Ion chromatography (IC), total organic carbon (TOC), and nitrite analysis are determined less than 24 hours after sampling. At each stage, sampling and analyses are performed with the greatest precaution to minimize all possible external contaminations, and the solutions are stored at 277 K under dark conditions. Hydroxyl radical formation rates ($R^f_{HO^\bullet}$) and polychromatic quantum yields ($\Phi_{HO^\bullet}$) are calculated using polychromatic wavelengths.

2.3 Physico-chemical measurements

Different parameters are monitored, including pH, conductivity and redox potential, which are measured using a Hanna multiparameter instrument. The UV-Vis spectrum of the collected cloud water is determined with an Agilent Technologies Cary 60 UV-vis spectrophotometer. The TOC concentration is determined with a TOC 5050A analyzer (Shimadzu). Hydrogen peroxide concentration is estimated using p-hydroxyphenilacetic acid (HPAA, purity > 98%) and horseradish peroxidase (POD) (solid containing 150-200 units per mg), according to the spectrofluorimetric quantification method (Miller and Kester, 2002). The formation of the dimer of HPAA is correlated with the concentration of hydrogen peroxide and is detected using a Varian Cary Eclipse Fluorescence Spectrophotometer setting excitation wavelengths at 320 nm, while emission is registered from 340 and 500 nm. The maximum signal is quantified at 408 nm. The scan rate is 600 nm min^{-1}, and a bandpass of 10 nm is set for excitation and emission. Nitrite ions concentration is determined by derivatization with 2,4-dinitrophenylhydrazine (DNPH) (purity > 97%), in acidic solution (HCl 37%). The UV-absorbing derivative (2,4-dinitrophenilazide) is detected by HPLC. The HPLC system (Waters Alliance) equipped with a diode array detector is used with an Eclipse XDB-C18 column (Agilent, 4.6 × 150 mm, 5 µm), and an isocratic method is adopted, using 40% acidified water (0.1% phosphoric acid) and 60% methanol. The flow rate is 1 mL min^{-1}, and 2,4-dinitrophenilazide is eluted with a retention time of 4.1 min (Kieber and Seaton, 1995) and detected at 307 nm. Fe(II) and Fe(III) concentrations are determined by the spectrophotometric method by complexation with ferrozine (purity > 97%), as described by Stookey (1970). Fe(II) and Fe(III) represent the oxidative state of the iron species. Adopted complexation method allows us to determine all Fe(II) and Fe(III) species present in solution (i.e., considered as free, aquacomplexes and as complex with other organic molecules). Ascorbic acid (purity reagent grade) is used as the reducing agent to determine total iron. The complex absorption is measured with a Varian Cary 300 Scan Spectrophotometer at 562 nm.

It has been previously demonstrated that filtration does not modify the soluble iron quantification in natural cloud water samples (Parazols et al., 2006; Vaitilingom et al., 2013).

It is not possible to measure particulate iron because the ferrozine method cannot solubilize solid phase iron (the contact time between acidic reagents and particulate iron is too short). Moreover, the iron particle is expected to be less reactive than the solubilized iron; consequently, its contribution can be neglected (Arakaki and Faust, 1998).

Ion chromatography (IC) analysis is performed employing a DIONEX DX-320 equipped with an IonPac AG11 (guard-column 4 × 50 mm) and an IonPac AS11 (analytical column 5 × 250 mm) for anions and a DIONEX ICS-1500 equipped with an IonPac CG16 (guard-column 4 × 50 mm) and an IonPac CS16 (analytical column 5 × 250 mm) for cations.

2.4 Statistical analysis

Principal component analysis (PCA) and hierarchical clustering analysis (HCA) are performed with R-3.1.2 software (R Core Team, 2013) using the FactoMineR package (version 1.28, (Lê et al., 2008). This statistical analysis provides a synthetic representation of experimental data as a function of the correlations between variables considered and similarities present among the analyzed samples. This technique allows the determination of information contained in a set of multivariate data, summarizing it in a few linear combinations of the variables (Deming et al., 1988). HCA data are grouped by similarity, considering all of the information contained in the data set. HCA is a statistical method to qualitatively study the composition of cloud water and can be used to identify the grouping variables that are not well detectable using only PCA.

2.5 Irradiation experiments

To evaluate the contribution of each possible photochemical source (nitrate, nitrite or hydrogen peroxide) to the hydroxyl radical formation in cloud water, synthetic solutions doped with a single source of oxidant are irradiated to quantify their contribution to the total generation of hydroxyl radicals in a more complex medium.

The photochemical device is composed of a Xenon lamp equipped with a water cooler to avoid the increase of temperature due to the infrared radiations and a mirror to reflect the light vertically. A Pyrex filter was located before the reactor for filtering of light at wavelengths below than 290 nm, corresponding to the lowest wavelengths of the solar emission spectrum. The reactor is a 40 mL cylindrical Pyrex container cooled by water circulation at a temperature of 278 ± 2 K to limit thermal reactions. Samples are continuously stirred with a magnetic stirrer using a Teflon bar to ensure homogeneity.

In Fig. 1, the emission spectrum of the lamp recorded using fiber optics coupled with a charge-coupled device (CCD) spectrophotometer (Ocean Optics USD 2000+UV-VIS) is reported. The energy was normalized with the actinometry results using a paranitroanisole (PNA)/pyridine actinometer (Dulin and Mill, 1982). Over the wavelength range of 290 to 600 nm, a total flux of 157 W m^{-2} is measured. The intensity values of the sun emission under clear sky and cloudy conditions at the puy de Dôme mountain in autumn 2013 are also presented in Fig. 1.

2.6 Hydroxyl radical formation rate and quantum yield determination

The hydroxyl radical formation rate is determined using terephthalate (TA) (terephthalic disodium salt, purity > 99%) as a probe (Charbouillot et al., 2011). Formation of hydroxyterephthalate (TAOH) is quantified using a Varian Cary Eclipse Fluorescence Spectrophotometer, setting excitation wavelengths at 320 nm, while the emission maximum is measured at 420 nm. The scan rate is 600 nm min^{-1}, and a bandpass of 10 nm is set for excitation and emission. Terephthalate is a useful probe because it allows the determination of hydroxyl radical formation rates in the presence of fluorescent dissolved organic matter. The concentration of the probe is in a large excess (2 mM) compared with the concentration of organic matter to trap all of the photogenerated hydroxyl radicals and then to estimate a value for the hydroxyl radical formation rate not affected by depletion of $HO^\bullet$ by other sinks.

The reaction between TA and the hydroxyl radical leads to the formation of fluorescent TAOH and non fluorescent secondary products (R1), as follows:

$$TA + HO^\bullet \rightarrow TAOH + products \qquad \text{(R1)}$$

The degradation rate of TA (R^d_{TA}) and formation rate of hydroxyl radical ($R^f_{HO^\bullet}$) and TAOH (R^f_{TAOH}) can be expressed as follows:

$$R^f_{HO^\bullet} \approx R^d_{TA} \approx \frac{R^f_{TAOH}}{\gamma} \qquad (1)$$

With

$$R^d_{TA} = k_{HO^\bullet,TA}\left[HO^\bullet\right][TA] \qquad (2)$$

where $k_{HO^\bullet,TA} = 4.0 \times 10^9$ M^{-1} s^{-1} is the second order rate constant of the reaction between HO$^\bullet$ and TA (Charbouillot et al., 2011), and [TA] is the initial concentration of terephthalate and γ is the TAOH formation yield calculated as a function of solution pH. This value is found to be linearly correlated with the pH value and is estimated between the values of 0.15 and 0.25 over the pH range of 4 to 7.

Other radicals, such as sulfate ($SO_4^{\bullet-}$) or chlorine/dichlorine ($Cl^\bullet/Cl_2^{\bullet-}$), can react with TA, leading to the H-abstraction as first chemical reaction. However, their direct generation is nearly exclusively due to the electron transfer reaction from the corresponding anion (*i.e.*, SO_4^{2-} and Cl^-, respectively) to the hydroxyl radical. Moreover, considering that the second order rate constant of aromatic compounds with the dichloride radical anion and the sulfate radical is expected to be one or two orders of magnitude lower than that with hydroxyl radical (Neta et al., 1988), and considering a relatively low concentration of sulfate and dichlorine radicals in our cloud samples, the TA reactivity can be attributed exclusively to the HO$^\bullet$.

The quantum yield of hydroxyl radical formation ($\Phi^{HO^\bullet}_{290\text{-}400nm}$) is defined as the ratio between the formation rate of HO$^\bullet$ ($R^f_{HO^\bullet}$) and the number of absorbed photons in Einstein per unit time in the overlap range of 290 to 600 (λ_1 and λ_2) (Eq. 3).

This value evaluates the photochemical process efficiency independent of the experimental photochemical conditions.

$$\Phi^{HO^\bullet}_{290-400nm} = \frac{R^f_{HO^\bullet}}{I_a} \qquad (3)$$

where I_a can be calculated from the following equation:

$$I_a = \int_{\lambda_1}^{\lambda_2} I_0(\lambda)(1-10^{-Abs(\lambda)})d\lambda \qquad (4)$$

where I_0 (photons m^{-2} s^{-1}) is the incident photon flux corresponding to the lamp emission and *Abs* is the absorption of cloud water (normalized considering the optical path length of 5 cm inside of the thermostated reactor).

2.7 Back-trajectory plots

Backward trajectories of collected air masses are calculated using the HYSPLIT (hybrid single-particle Lagrangian integrated trajectory) model with the GDAS1 meteorological data archive and the model of vertical velocity (*http://ready.arl.noaa.gov/HYSPLIT.php*). Backward trajectories are calculated for 72 hours (Draxler and Rolph, 2012).

2.8 Model description

The M2C2 combines detailed multiphase chemistry along with the parameterization of the microphysics (Leriche et al., 2001; Leriche et al., 2000; Deguillaume et al., 2004). Particularly, the detailed chemistry of H_xO_y, chlorine, carbonates, NO_y, sulfur, transition metal ions (iron, copper, manganese) and the oxidation of volatile organic compounds (VOCs) is included. Photolysis rates are calculated in the gaseous and aqueous phases, and the pH is calculated following the H^+ concentration. Numerical results consist of following the time evolution of the concentrations of each chemical species and calculating at each time step the relative contribution of chemical reactions in the production/destruction of chemical compounds.

In this study, a simplified version of the model is used. The cloud chemical mechanism is restricted to inorganic chemistry (H_xO_y, nitrogen, iron) that leads to the $HO^\bullet$ formation (see Table SM1 for details about the considered reactions). The complexation of iron by oxalate is also considered in the model because it can interfere with the $HO^\bullet$ formation rates (Long et al., 2013). Laboratory irradiation experiments are simulated with the M2C2 model considering its chemical module and neglecting microphysical processes and mass transfer parameterizations. Temperature and pH remained constant during the simulation time. We set the pH for each cloud water sample to the values reported in Table SM2, and the temperature is fixed at 278 K, which corresponds to the temperature of the irradiated solutions. The simulated irradiation intensity is held constant and homogenous throughout the experiment. The actinic flux of the experimental lamp is discretized in the tropospheric ultraviolet-visible (TUV) model in 156 non-regular intervals over a wavelength range of 120 to 750 nm (Madronich and Flocke, 1999). The photolysis rates of the chemical species are calculated in TUV according to the experimental quantum yields and absorption cross-sections and are indicated in Table SM1. Experimental chemical concentrations (Table SM2) are used to initialize the model (H_2O_2, nitrite, nitrate, iron). Moreover, oxalic acid is considered as an organic complexant during the Fe(II)/Fe(III) cycle. The formation rate of $HO^\bullet$ is calculated by the model considering the modeled contribution of each reaction producing $HO^{\bullet}$ during one hour of experiment.

3 Results and Discussion

3.1 Classification of cloud samples

Recently, physicochemical parameters and concentrations of the major organic and inorganic compounds of cloud samples collected over the last ten years at the puy de Dôme are measured and statistically analyzed by PCA (Deguillaume et al., 2014). Along with the corresponding back-trajectory plots, 4 different categories of air masses reaching the summit of the PUY could be distinguished, as follows: polluted, continental, marine and highly marine. Highly marine clouds exhibited high concentrations of Na^+ and Cl^-, and the marine category presented a lower concentration of ions but more elevated pH, while the two remaining clusters, classified as “continental” and “polluted”, are characterized by the second-highest and highest levels of NH_4^+, NO_3^-, and SO_4^{2-}, respectively.

In Table SM2, the measured physico-chemical composition of the cloud water samples is reported for this study. We use the same statistical analysis to classify these cloud water samples as Deguillaume et al. (2014). PCA is performed using the pH and the concentration of sulfate, nitrate, chloride, sodium and ammonium ions as variables. Fig. 2 reports the scores plot for samples used for the previously reported classification as a function of the attributed class and for the new samples. Three types are identified, as follows: (*i*) highly marine, (2 samples) characterized by pH values of 5.0 and 5.6, respectively, high concentration of chloride and sodium and low concentrations of nitrate, nitrite and ammonium; (*ii*) marine cloud waters (28 samples), showing pH values between 4.7 and 7.6 and very low concentrations of anions and cations, and (*iii*) continental samples (11 samples), with pH values from 4.1 to 6.9 and a medium concentration of nitrates, sulfates and ammonium, while sodium and chloride concentrations are very low. No sample could be classified as polluted cloud water because polluted cloud waters have been characterized by concentrations of nitrates, sulfates and ammonium higher than 350, 70 and 330 µM, respectively. This statistical analysis confirms that the majority of the collected samples are of marine origin. This statistical analysis is confirmed by the back-trajectory plots from the HYSPLIT model, showing that most of the air masses reaching the puy de Dôme arises from the west sector *i.e.*, from the Atlantic Ocean.

3.2 Determination of the hydroxyl radical formation rates and photolysis rates

The concentration of the main photochemical sources of $HO^{\bullet}$ for each sample is reported in Table 1. Particularly, the Fe(II) and Fe(III) concentrations are below the detection limit (0.01 µM) for the majority of the collected samples. The highest value found for the Fe(II) concentration is 0.7 µM, while it is 0.6 µM for Fe(III), corresponding to typical values found for marine origin cloud waters (Parazols et al., 2006). The H_2O_2 concentration values range between 6 and 50 µM, nitrate is evaluated between 2 and 220 µM, while the nitrite concentration is between 0 and 1.4 µM.

The $R^{f}_{HO^{\bullet}}$ was measured in pure water doped with different concentrations of hydrogen peroxide, nitrate and nitrite on the same order of magnitude as the collected natural samples. The conditions were those used for natural cloud samples (see Sect. 2.6). A linear correlation between $R^{f}_{HO^{\bullet}}$ and the concentrations of photochemical precursors is found (Fig. 3). The photolysis rate (J) (s^{-1}) is then estimated from the slopes and are reported in Table 4. For H_2O_2, the J value is half of the experimental slope because H_2O_2 provides two $HO^{\bullet}$ radicals.

The hydroxyl radical formation rate ($R^{f}_{HO^{\bullet}}$) is determined for 36 samples, and its value is estimated between 3.3×10^{-12} and 4.2×10^{-10} M s^{-1}. Higher values are obtained for cloud water samples of continental origin, while the values found for marine and highly marine cloud waters are less than 1.4×10^{-10} M s^{-1}. The quantum yield of the formation of hydroxyl radicals under polychromatic irradiation between 290 and 400 nm ($\Phi^{HO^{\bullet}}_{290\text{-}400nm}$, see eq.(3)) is estimated as between 10^{-5} and 10^{-2}. (Table 2).

To our knowledge, only a scarce number of data are available in the literature concerning measurements of hydroxyl radical formation rates ($R^{f}_{HO^{\bullet}}$) and formation quantum yield ($\Phi^{HO^{\bullet}}$) in real cloud waters (Table 3). Faust and Allen (1993) measured the photoformation rates of $HO^{\bullet}$ (ranging from 1.3 to 8.3×10^{-10} M s^{-1}) under monochromatic light (313 nm) and hydroxyl radical quantum yield (between ~ 5×10^{-4} and 10^{-2}) of six continental cloud water samples. Anastasio and McGregor (2001) investigated the photoreactivity of two cloud waters from the Tenerife Islands to compare the obtained values with fog waters. The authors found

$R^f_{HO^\bullet}$ ranging between 3.0 and 6.9 × 10^{-10} M s^{-1} that are approximately 1 order of magnitude higher than those reported in this study for marine cloud waters, and the differences can be attributed to the air mass origin, as suggested by Faust and Allen (1993). The authors suggested that long-range terrestrial aerosol and gas transport in continental clouds could provide an additional source of hydroxyl radicals compared with other marine or remote clouds.

3.3 Modeling the hydroxyl radical formation rates

We simulate the hydroxyl formation rate, $R^f_{HO^\bullet}$ mod, using the model along with the relative contribution (%) of each chemical source (Table SM3). In Fig. 4, the differences between the modeled and experimental $HO^\bullet$ formation rates are estimated calculating the bias error (($R^f_{HO^\bullet}$ mod - $R^f_{HO^\bullet}$ exp) / $R^f_{HO^\bullet}$ exp in (%)). Globally, for the whole cloud water samples (black boxplot), the model can reproduce the range of measured hydroxyl radical formation rates with a slight model underestimation (median of the bias error equal to -23%). However, if the cloud samples are discretized as a function of different iron concentration ranges (boxplots in color), then the model tends to overestimate the hydroxyl radicals formation for iron concentrations (Fe(II) + Fe(III)) more than 0.1 µM. For concentration of iron between 0.1 and 0.4 µM (8 cloud samples), the median of the bias error is 61% whereas for iron concentrations over 0.4 µM (5 cloud samples), the median reaches 260%. For cloud samples in which the iron concentration is 0.4 µM, the modeled contribution to the hydroxyl radical formation of iron (Fenton reaction and photolysis of aqua-complexes) can reach 80% (Table SM3). In the model, Fe(III) is partially complexed with oxalic acid, but the majority of iron for these cloud samples is simulated as aqua-complexes (mainly $Fe(OH)^{2+}$ and $Fe(OH)_2^{+}$). Therefore, iron can act as a significant $HO^\bullet$ source due to its efficient photolysis (Reactions R7, R8, R9, Table SM1) and the Fenton reaction with H_2O_2 (Reactions R11, Table SM1).

However, in atmospheric natural water, the chemical composition of organic matter is still not very well characterized (Herckes et al., 2013). Part of this organic matter is expected to efficiently complex metals in cloud water (Okochi and Brimblecombe, 2002). Due to missing information about the iron speciation and complexation in natural cloud water, the model probably overestimates the free Fe(III). Moreover, iron organic complexes are not expected to directly generate hydroxyl radicals but primarily contribute to the oxidative capacity *via*

Fe(II) generation and the Fenton process. To evaluate this hypothesis, we decide to consider the iron as totally complexed by the organic matter present in natural cloud waters. As a first general approximation, we consider iron as not reactive in the model. The new simulations show that the majority of the simulated values (75%) of the hydroxyl radical formation rates are now underestimated by the model (median of the bias error equal to -40%) (Fig. 5).

Based on the laboratory irradiation experiments (sec. 2.6 and Fig. 3), new photolysis rates from nitrite, nitrate and hydrogen peroxide are previously estimated from the hydroxyl radical formation rates (Table 4). For nitrate and H_2O_2, the values calculated by the model are lower than the experimental ones; the experimental photolysis rates are higher by a factor ~1.5 for H_2O_2 and ~2 for nitrate. For nitrite, the experimental photolysis rate is approximately half of the modeled value. These discrepancies should partially explain the underestimation of $HO^\bullet$ formation by the model. Therefore, we consider the experimental photolysis rates in the model, and a new comparison of modeled $HO^\bullet$ formation rates with experimental values is shown in Fig. 5. The median of the bias error is -3% with the 25th and 75th percentiles at -50 and 60%, respectively. Table SM4 reports the distribution of the relative contributions of H_2O_2, NO_3^- and NO_2^- photolysis to the modeled $R^f_{HO^\bullet}$. While the median value of the nitrite and nitrate contributions is calculated by the model as equal to 1 and 5%, respectively (Fig. 6), the main $HO^\bullet$ contributor is H_2O_2 photolysis (median value of 93%, with the 25th and 75th percentiles at 85 and 96%, respectively). This result suggests that H_2O_2 is the key compound that drives the oxidative capacity of our cloud water samples when iron concentrations are relatively low or when iron is suggested to be totally complexed by organic matter.

4 Conclusion

In this study, we compare experimental and modeled $HO^\bullet$ formation rates for 41 cloud water samples with contrasted chemical compositions depending on the origin of the air masses. This approach helps to elucidate the complex aqueous photoreactivity of natural cloud water that is expected to drive the oxidative capacity. Experimental data are obtained considering only the $HO^\bullet$ formation sources with addition of an excess of chemical probe leading to the measurements of total generated $HO^\bullet$ radicals. The first comparison with the M2C2 model shows that the model can reproduce the order of magnitude of measured $R^f_{HO^\bullet}$ (from 1.1×10^{-11} to 4.2×10^{-10} M s^{-1} and from 1.1×10^{-11} to 2.4×10^{-10} M s^{-1} for experimental and modeled values, respectively). Some discrepancies appear for samples containing iron concentrations over 0.4 µM in which the model overestimates the contribution of iron(III)-aqua complexes to the $HO^\bullet$ production rate. Ultimately, the aqueous chemical mechanism in the model was modified considering new photolysis rates for H_2O_2, nitrite and nitrate estimated by laboratory irradiation experiments. As a sensitivity test, iron reactivity was also suppressed in the model to account for the total complexation of iron. The modeled production rates of $HO^\bullet$ with the updated mechanism are closer to the experimental values. This supports the hypothesis that iron could be strongly complexed by the organic matter in natural cloud water. These complexes could be more stable and less photoreactive, leading to less $HO^\bullet$ production than that calculated by theoretical models in which only the photochemistry of Fe(III)-carboxylate is considered (Weller et al., 2014). In this context, evaluation of the complexation of iron by organic compounds in the cloud aqueous phase and the photoreactivity of these complexes should be pursued in the future. Their photoreactivity provides significant data to understand the specific role of iron species and, more generally, the oxidant capacity of this medium.

Acknowledgments. The authors acknowledge the financial support from the Regional Council of Auvergne, from the Observatoire de Physique du Globe de Clermont-Ferrand (OPGC), from the "Fédération de Recherche en Environnement" through the CPER "Environnement" founded by the "Région Auvergne", the French ministry, FEDER from the European community. This work on the analysis of the cloud water chemical composition is supported by the French Ministry and CNRS-INSU. The authors are very grateful to the Agence Nationale de la Recherche (ANR) for its financial support through the BIOCAP project (ANR-13-BS06-0004) and CUMULUS project (ANR-10-BLAN-0617).

References

Albinet, A., Minero, C., and Vione, D.: Photochemical generation of reactive species upon irradiation of rainwater: Negligible photoactivity of dissolved organic matter, Sci. Total Environ., 408, 3367-3373, 2010.

Altieri, K. E., Seitzinger, S. P., Carlton, A. G., Turpin, B. J., Klein, G. C., and Marshall, A. G.: Oligomers formed through in-cloud methylglyoxal reactions: chemical composition, properties, and mechanisms investigated by ultra-high resolution FT-ICR mass spectrometry, Atmos. Environ., 42, 1476-1490, 2008.

Anastasio, C., and McGregor, K. G.: Chemistry of fog waters in California's Central Valley: 1. In situ photoformation of hydroxyl radical and singlet molecular oxygen, Atmos. Environ., 35, 1079-1089, 2001.

Arakaki, T., and Faust, B. C.: Sources, sinks, and mechanisms of hydroxyl radical (OH) photoproduction and consumption in authentic acidic continental cloud waters from Whiteface Mountain, New York: The role of the Fe(r) (r = II, III) photochemical cycle, J. Geophys. Res., 103, 3487-3504, 10.1029/97jd02795, 1998.

Arakaki, T., Kuroki, Y., Okada, K., Nakama, Y., Ikota, H., Kinjo, M., Higuchi, T., Uehara, M., and Tanahara, A.: Chemical composition and photochemical formation of hydroxyl radicals in aqueous extracts of aerosol particles collected in Okinawa, Japan, Atmos. Environ., 40, 4764-4774, 2006.

Arakaki, T., Anastasio, C., Kuroki, Y., Nakajima, H., Okada, K., Kotani, Y., Handa, D., Azechi, S., Kimura, T., Tsuhako, A., and Miyagi, Y.: A general scavenging rate constant for reaction of hydroxyl radical with organic carbon in atmospheric waters, Environ. Sci. Technol., 47, 8196-8203, 10.1021/es401927b, 2013.

Brantner, B., Fierlinger, H., Puxbaum, H., and Berner, A.: Cloudwater chemistry in the subcooled droplet regime at Mount Sonnblick (3106 m a.s.l., Salzburg, Austria), Water, Air, & Soil Pollution, 74, 363-384, 10.1007/bf00479800, 1994.

Carlton, A. G., Turpin, B. J., Altieri, K. E., Seitzinger, S., Reff, A., Lim, H.-J., and Ervens, B.: Atmospheric oxalic acid and SOA production from glyoxal: results of aqueous photooxidation experiments, Atmos. Environ., 41, 7588-7602, 2007.

Charbouillot, T., Brigante, M., Mailhot, G., Maddigapu, P. R., Minero, C., and Vione, D.: Performance and selectivity of the terephthalic acid probe for OH as a function of temperature, pH and composition of atmospherically relevant aqueous media, J. Photochem. Photobiol., A, 222, 70-76, 10.1016/j.jphotochem.2011.05.003, 2011.

Charbouillot, T., Gorini, S., Voyard, G., Parazols, M., Brigante, M., Deguillaume, L., Delort, A.-M., and Mailhot, G.: Mechanism of carboxylic acid photooxidation in atmospheric aqueous phase: Formation, fate and reactivity, Atmos. Environ., 56, 1-8, http://dx.doi.org/10.1016/j.atmosenv.2012.03.079, 2012.

De Haan, D. O., Tolbert, M. A., and Jimenez, J. L.: Atmospheric condensed-phase reactions of glyoxal with methylamine, Geophys. Res. Lett., 36, L11819, 10.1029/2009gl037441, 2009.

Deguillaume, L., Leriche, M., Monod, A., and Chaumerliac, N.: The role of transition metal ions on HOx radicals in clouds: a numerical evaluation of its impact on multiphase chemistry, Atmos. Chem. Phys., 4, 95-110, 10.5194/acp-4-95-2004, 2004.

Deguillaume, L., Leriche, M., Desboeufs, K., Mailhot, G., George, C., and Chaumerliac, N.: Transition metals in atmospheric liquid phases: sources, reactivity, and sensitive parameters, Chem. Rev., 105, 3388-3431, doi:10.1021/cr040649c, 2005.

Deguillaume, L., Charbouillot, T., Joly, M., Vaitilingom, M., Parazols, M., Marinoni, A., Amato, P., Delort, A. M., Vinatier, V., Flossmann, A., Chaumerliac, N., Pichon, J. M., Houdier, S., Laj, P., Sellegri, K., Colomb, A., Brigante, M., and Mailhot, G.: Classification of clouds sampled at the puy de Dôme (France) based on 10 yr of monitoring of their physicochemical properties, Atmos. Chem. Phys., 14, 1485-1506, 10.5194/acp-14-1485-2014, 2014.

Deming, S. N., Michotte, Y., Massart, D. L., Kaufman, L., and Vandeginste, B. G. M.: Chemometrics: A textbook, 1st Edition, Elsevier Science, http://dx.doi.org/10.1016/0169-7439(89)80019-X, 1988.

HYSPLIT (HYbrid Single-particle Lagrangian Integrated Trajectory) Model Access via NOAA ARL READY Website, available at: http://ready.arl.noaa.gov/ HYSPLIT.php, 2012.

Dulin, D., and Mill, T.: Development and evaluation of sunlight actinometers, Environ. Sci. Technol., 16, 815-820, 10.1021/es00105a017, 1982.

Ervens, B., and Volkamer, R.: Glyoxal processing by aerosol multiphase chemistry: towards a kinetic modeling framework of secondary organic aerosol formation in aqueous particles, Atmos. Chem. Phys., 10, 8219-8244, 10.5194/acp-10-8219-2010, 2010.

Ervens, B., Turpin, B. J., and Weber, R. J.: Secondary organic aerosol formation in cloud droplets and aqueous particles (aqSOA): a review of laboratory, field and model studies, Atmos. Chem. Phys., 11, 11069-11102, 10.5194/acp-11-11069-2011, 2011.

Ervens, B., Sorooshian, A., Lim, Y. B., and Turpin, B. J.: Key parameters controlling OH-initiated formation of secondary organic aerosol in the aqueous phase (aqSOA), J. Geophys. Res., [Atmos.], 119, 3997-4016, 10.1002/2013jd021021, 2014.

Faust, B. C., and Allen, J. M.: Aqueous-phase photochemical formation of hydroxyl radical in authentic cloudwaters and fogwaters, Environ. Sci. Technol., 27, 1221-1224, doi:10.1021/es00043a024, 1993.

Herckes, P., Valsaraj, K. T., and Collett Jr, J. L.: A review of observations of organic matter in fogs and clouds: Origin, processing and fate, Atmos. Res., 132-133, 434-449, http://dx.doi.org/10.1016/j.atmosres.2013.06.005, 2013.

Herrmann, H., Hoffmann, D., Schaefer, T., Bräuer, P., and Tilgner, A.: Tropospheric aqueous-phase free-radical chemistry: radical sources, spectra, reaction kinetics and prediction tools, ChemPhysChem, 11, 3796-3822, 10.1002/cphc.201000533, 2010.

Hervo, M.: Etude des propietés optiques et radiatives des aérosols en atmosphère réelle: Impact de l'hydroscopicité. PhD thesis, Blaise Pascal University, Aubiere, 2013.

Kieber, R. J., and Seaton, P. J.: Determination of subnanomolar concentrations of nitrite in natural waters, Anal. Chem., 67, 3261-3264, 10.1021/ac00114a024, 1995.

Lê, S., Josse, J., and Husson, F.: FactoMineR: An R Package for Multivariate Analysis, J. Stat. Softw., 25, 1-18, 2008.

Leriche, M., Voisin, D., Chaumerliac, N., Monod, A., and Aumont, B.: A model for tropospheric multiphase chemistry: application to one cloudy event during the CIME experiment, Atmos. Environ., 34, 5015-5036, http://dx.doi.org/10.1016/S1352-2310(00)00329-0, 2000.

Leriche, M., Chaumerliac, N., and Monod, A.: Coupling quasi-spectral microphysics with multiphase chemistry: a case study of a polluted air mass at the top of the Puy de Dôme mountain (France), Atmos. Environ., 35, 5411-5423, http://dx.doi.org/10.1016/S1352-2310(01)00300-4, 2001.

Long, Y., Charbouillot, T., Brigante, M., Mailhot, G., Delort, A.-M., Chaumerliac, N., and Deguillaume, L.: Evaluation of modeled cloud chemistry mechanism against laboratory irradiation experiments: The HxOy/iron/carboxylic acid chemical system, Atmos. Environ., 77, 686-695, http://dx.doi.org/10.1016/j.atmosenv.2013.05.037, 2013.

Madronich, S., and Flocke, S.: The Role of Solar Radiation in Atmospheric Chemistry, in: Environmental Photochemistry, edited by: Boule, P., The Handbook of Environmental Chemistry, Springer Berlin Heidelberg, 1-26, 1999.

Miller, W. L., and Kester, D. R.: Hydrogen peroxide measurement in seawater by (p-hydroxyphenyl)acetic acid dimerization, Anal. Chem., 60, 2711-2715, 10.1021/ac00175a014, 2002.

Neta, P., Huie, R. E., and Ross, A. B.: Rate constants for reactions of inorganic radicals in aqueous solution, J. Phys. Chem. Ref. Data, 17, 1027-1284, doi:http://dx.doi.org/10.1063/1.555808, 1988.

Okochi, H., and Brimblecombe, P.: Potential trace metal-organic complexation in the atmosphere, Sci. World J., 2, 10.1100/tsw.2002.132, 2002.

Parazols, M., Marinoni, A., Amato, P., Abida, O., Laj, P., and Mailhot, G.: Speciation and role of iron in cloud droplets at the puy de Dome station, J. Atmos. Chem., 54, 267-281, 10.1007/s10874-006-9026-x, 2006.

Perri, M. J., Seitzinger, S., and Turpin, B. J.: Secondary organic aerosol production from aqueous photooxidation of glycolaldehyde: Laboratory experiments, Atmos. Environ., 43, 1487-1497, http://dx.doi.org/10.1016/j.atmosenv.2008.11.037, 2009.

R: a language and invironment for statistical computing R. foundation for Statistical Computing http://www.R-project.org/, 2013.

Seinfeld, J. H., and Pandis, S. N.: Atmospheric Chemistry and Physics: From Air Pollution to Climate Change, 2nd Edition, 2006.

Stookey, L. L.: Ferrozine - a new spectrophotometric reagent for iron, Anal. Chem., 42, 779-781, doi:10.1021/ac60289a016, 1970.

Tan, Y., Lim, Y. B., Altieri, K. E., Seitzinger, S. P., and Turpin, B. J.: Mechanisms leading to oligomers and SOA through aqueous photooxidation: insights from OH radical oxidation of acetic acid and methylglyoxal, Atmos. Chem. Phys., 12, 801-813, 10.5194/acpd-11-18319-2011, 2011.

Tilgner, A., and Herrmann, H.: Radical-driven carbonyl-to-acid conversion and acid degradation in tropospheric aqueous systems studied by CAPRAM, Atmos. Environ., 44, 5415-5422, http://dx.doi.org/10.1016/j.atmosenv.2010.07.050, 2010.

Vaitilingom, M., Deguillaume, L., Vinatier, V., Sancelme, M., Amato, P., Chaumerliac, N., and Delort, A.-M.: Potential impact of microbial activity on the oxidant capacity and organic carbon budget in clouds, Proc. Natl. Acad. Sci., 110, 559-564, 10.1073/pnas.1205743110, 2013.

Weller, C., Tilgner, A., Brauer, P., and Herrmann, H.: Modeling the impact of iron-carboxylate photochemistry on radical budget and carboxylate degradation in cloud droplets and particles, Environ. Sci. Technol., 48, 5652-5659, 10.1021/es4056643, 2014.

Yu, X.-Y., and Barker, J. R.: Hydrogen peroxide photolysis in acidic aqueous solutions containing chloride ions. II. Quantum yield of HO(aq) radicals, J. Phys. Chem. A, 107, 1325-1332, 10.1021/jp026666s, 2003.

Zafiriou, O. C., and Bonneau, R.: Wavelength-dependent quantum yield of OH radical formation from photolysis of nitrite ions in water, Photochem. Photobiol., 45, 723-727, 10.1111/j.1751-1097.1987.tb07873.x, 1987.

Zellner, R., Exner, M., and Herrmann, H.: Absolute OH quantum yields in the laser photolysis of nitrate, nitrite and dissolved H_2O_2 at 308 and 351 nm in the temperature range 278–353 K, J. Atmos. Chem., 10, 411-425, 10.1007/bf00115783, 1990.

Table Caption

Table 1. Concentration of main sources of hydroxyl radical in sampled clouds. 41 samples have been analyzed. BDL: below detection limit (0.01 µM for iron and 0.05 µM for NO_2^-), NM: not measured.

Table 2. Hydroxyl radical formation rate ($R^f_{HO^\bullet}$)and hydroxyl radical polychromatic quantum yield formation ($\Phi_{HO^\bullet}$ $_{(290\text{-}400nm)}$) values estimated from cloud water samples. NM: not measured. Mar: Marine, H-Mar: highly marine and Cont: continental influence. The error on $R^f_{HO^\bullet}$ are derived at the 1-σ level simply from the scattering of experimental data.

Table 3. Hydroxyl radical formation rates ($R^f_{HO^\bullet}$) and polychromatic quantum yield ($\Phi_{HO^\bullet}$)found in literature and in this work.

Table 4. Modeled photolysis rates calculated by the model *versus* experimental photolysis rates obtained from experiments reported in Fig. 3.

Table 1. Concentration of main sources of hydroxyl radical in sampled clouds. 41 samples have been analyzed. BDL: below detection limit (0.01 µM for iron and 0.05 µM for NO_2^-), NM: not measured.

Sample	Iron (µM)		H_2O_2 (µM)	NO_3^- (µM)	NO_2^- (µM)
	II	III			
1	NM	NM	12.3	16.7	0.46
2	NM	NM	9.0	6.1	1.44
3	NM	NM	15.1	9.9	0.40
4	NM	NM	14.0	14.2	0.30
5	NM	NM	13.0	14.7	0.38
6	NM	NM	7.8	2.6	BDL
7	NM	NM	6.2	1.7	BDL
8	NM	NM	9.7	6.9	BDL
9	NM	NM	8.2	8.2	BDL
10	NM	NM	10.2	2.3	BDL
11	NM	NM	17.2	5.6	BDL
12	BDL	0.57	18.0	24.7	0.28
13	BDL	0.12	24.6	23.7	1.10
14	BDL	0.11	12.0	19.0	BDL
15	BDL	BDL	14.5	19.0	0.23
16	BDL	BDL	9.1	21.3	0.10
17	BDL	0.11	16.2	219.6	0.05
18	0.10	0.01	16.2	205.6	0.07
19	BDL	BDL	14.9	20.0	0.12
20	BDL	BDL	15.7	37.4	0.19
21	BDL	BDL	22.2	72.6	0.42
22	BDL	BDL	52.3	131.9	0.72
23	BDL	BDL	49.4	133.1	0.95
24	BDL	BDL	8.1	7.5	BDL
25	0.08	0.02	6.7	21.2	0.15
26	0.40	0.20	6.8	39.7	BDL
27	0.70	0.20	6.6	75.6	BDL
28	0.70	0.30	7.2	73.8	BDL
29	0.01	0.10	8.0	24.7	0.27
30	BDL	0.16	8.8	19.7	0.52
31	BDL	0.45	9.1	20.7	0.61
32	BDL	BDL	13.1	21.4	0.07
33	BDL	0.10	2.1	6.1	BDL
34	0.09	BDL	8.4	10.3	0.47
35	BDL	BDL	2.2	15.1	0.51
36	BDL	0.03	2.1	20.3	BDL
37	BDL	0.03	2.1	18.5	BDL
38	0.07	BDL	2.4	13.5	0.34
39	0.04	BDL	3.1	20.8	BDL
40	BDL	0.01	5.7	39.1	BDL
41	BDL	0.02	5.3	46.5	0.16

Table 2. Hydroxyl radical formation rate ($R^{f}_{HO^{\bullet}}$ (M s^{-1})) and hydroxyl radical polychromatic quantum yield formation ($\Phi_{HO^{\bullet}\,(290\text{-}400nm)}$) values estimated from cloud water samples. NM: not measured. Mar: Marine, H-Mar: highly marine and Cont: continental influence. The error on $R^{f}_{HO^{\bullet}}$ are derived at the 1-σ level simply from the scattering of experimental data.

Sample	$R^{f}_{HO^{\bullet}}$ (M s^{-1})	$\Phi^{290-400nm}_{HO^{\bullet}}$	Class	Sample	$R^{f}_{HO^{\bullet}}$ (M s^{-1})	$\Phi^{290-400nm}_{HO^{\bullet}}$	Class
1	$(3.30\pm0.23)\times10^{-11}$	1.27×10^{-3}	Mar	22	$(3.37\pm0.01)\times10^{-10}$	2.5×10^{-3}	Cont
2	NM	NM	Mar	23	$(4.16\pm0.01)\times10^{-10}$	1.8×10^{-3}	Cont
3	NM	NM	Mar	24	$(5.10\pm0.01)\times10^{-10}$	NM	Mar
4	$(1.40\pm0.01)\times10^{-10}$	1.0×10^{-2}	H-Mar	25	$(2.42\pm0.08)\times10^{-11}$	1.9×10^{-4}	Cont
5	$(1.24\pm0.02)\times10^{-10}$	6.0×10^{-3}	H-Mar	26	$(1.41\pm0.01)\times10^{-10}$	3.4×10^{-3}	Cont
6	$(2.77\pm0.01)\times10^{-11}$	1.5×10^{-4}	Mar	27	$(4.95\pm0.01)\times10^{-11}$	1.5×10^{-4}	Cont
7	$(5.60\pm0.06)\times10^{-11}$	9.0×10^{-3}	Mar	28	NM	NM	Cont
8	$(2.48\pm0.01)\times10^{-11}$	2.9×10^{-3}	Mar	29	$(8.48\pm0.04)\times10^{-11}$	1.3×10^{-4}	Mar
9	$(2.20\pm0.02)\times10^{-11}$	1.8×10^{-3}	Mar	30	$(8.43\pm0.02)\times10^{-11}$	1.2×10^{-4}	Mar
10	$(2.93\pm0.02)\times10^{-11}$	2.4×10^{-3}	Mar	31	$(6.11\pm0.21)\times10^{-11}$	5.1×10^{-5}	Mar
11	$(6.77\pm0.02)\times10^{-11}$	2.7×10^{-3}	Mar	32	NM	NM	Mar
12	$(6.10\pm0.19)\times10^{-11}$	1.7×10^{-4}	Mar	33	$(3.27\pm0.23)\times10^{-12}$	1.3×10^{-5}	Mar
13	$(4.66\pm0.01)\times10^{-11}$	1.5×10^{-4}	Mar	34	$(2.73\pm0.01)\times10^{-11}$	8.5×10^{-4}	Mar
14	$(2.81\pm0.01)\times10^{-11}$	2.0×10^{-4}	Mar	35	$(3.60\pm0.30)\times10^{-11}$	6.0×10^{-4}	Mar
15	$(1.09\pm0.04)\times10^{-11}$	9.0×10^{-5}	Mar	36	$(5.97\pm0.12)\times10^{-11}$	9.6×10^{-5}	Mar
16	NM	NM	Mar	37	$(2.41\pm0.04)\times10^{-11}$	8.4×10^{-5}	Mar
17	$(6.05\pm0.44)\times10^{-11}$	4.1×10^{-5}	Cont	38	$(5.76\pm0.13)\times10^{-11}$	2.7×10^{-4}	Mar
18	$(3.39\pm0.20)\times10^{-11}$	3.2×10^{-5}	Cont	39	$(2.69\pm0.04)\times10^{-11}$	1.1×10^{-4}	Mar
19	$(8.11\pm0.02)\times10^{-11}$	1.9×10^{-4}	Mar	40	$(1.27\pm0.01)\times10^{-10}$	2.6×10^{-4}	Cont
20	$(8.46\pm0.01)\times10^{-11}$	8.4×10^{-3}	Mar	41	$(1.09\pm0.01)\times10^{-10}$	5.1×10^{-4}	Cont
21	$(1.54\pm0.01)\times10^{-10}$	1.5×10^{-3}	Cont				

Table 3. Hydroxyl radical formation rates ($R^{f}_{HO^\bullet}$, M s^{-1})and polychromatic quantum yield ($\Phi_{HO^\bullet}$)found in literature and in this work.

	$R^{f}_{HO^\bullet}$ (M s^{-1})	$\Phi_{^\bullet OH}$	References
Rain water	2.0 - 6.5 × 10^{-11}		(Albinet et al., 2010)
Cloud water	1.3 - 8.3 × 10^{-10}	4.6 × 10^{-4} - 1.0 × 10^{-2} at 313 nm	(Faust and Allen, 1993)
Fog	0.9 - 6.9 × 10^{-10}		
Aqueous extracted aerosol particles	0.4 - 3.8 × 10^{-10}	3.0 × 10^{-4} - 1.7 × 10^{-3}	(Arakaki et al., 2006)
Cloud water	3.1 - 6.9 × 10^{-10}		(Anastasio and McGregor, 2001)
Cloud water	0.3 - 5.9 × 10^{-10}	5.1 × 10^{-4} - 3.0 × 10^{-3}	(Arakaki and Faust, 1998)
Cloud water at the PUY station	0.2 - 4.2 × 10^{-10}	1.3 × 10^{-5} - 1.0 × 10^{-2} Polychromatic	This work

Table 4. Modeled photolysis rates calculated by the model *versus* experimental photolysis rates obtained from experiments reported in Fig. 3.

	Modeled photolysis rates J (s^{-1})	Experimental photolysis rates J (s^{-1})
$H_2O_2 \xrightarrow{h\nu} 2HO^\bullet$	1.52×10^{-6}	$(2.50 \pm 0.11) \times 10^{-6}$
$HNO_2 \xrightarrow{h\nu} HO^\bullet + NO^\bullet$	6.16×10^{-5}	
$NO_2^- + H_2O \xrightarrow{h\nu} HO^\bullet + NO^\bullet + HO^-$	9.98×10^{-6}	$(5.15 \pm 0.30) \times 10^{-6}$
$NO_3^- + H_2O \xrightarrow{h\nu} HO^\bullet + NO_2^\bullet + HO^-$	6.71×10^{-8}	$(1.23 \pm 0.04) \times 10^{-7}$
$Fe^{3+} + H_2O \xrightarrow{h\nu} HO^\bullet + Fe^{2+} + H^+$	1.24×10^{-6}	
$Fe(OH)^{2+} \xrightarrow{h\nu} HO^\bullet + Fe^{2+}$	2.81×10^{-4}	
$Fe(OH)_2^+ \xrightarrow{h\nu} HO^\bullet + Fe^{2+} + HO^-$	3.53×10^{-4}	

Figure Caption

Fig. 1. Absorption spectra of different cloud water samples (left axis) and the right-hand axis shows the emission spectrum of the adopted Xenon lamp reaching solutions over the range of 290 to600 nm (total flux intensity = 157 W m^{-2}) compared with the sun emission spectrum (dashed line) for a sunny (353 W m^{-2}) and a cloudy day (90 W m^{-2}) in October 2013.

Fig. 2. Scores plot obtained by PCA analysis of 137 samples (corresponding to 73 cloud events) collected before 2013 and grouped in four classes in function of previously described classification (Deguillaume et al., 2014) and 41 samples (numbered from 80 to 120) collected during 2013 and 2014. These new data correspond to 15 cloud events and are indicated in black triangles. Statistical analysis is performed using 6 selected variables (pH, [Na^+], [Cl^-], [SO_4^{2-}], [NO_3^-], and [NH_4^+]). The scree plot obtained from autoscaled data shows that two selected principal components (PC) containing a total variance of about 81%.

Fig. 3. Scatter plot of hydroxyl radical formation rates *vs.* hydrogen peroxide, nitrate and nitrite concentrations using 2 mM of TA at pH 5.0 under Xenon lamp irradiation. The solid line is the linear fit, and dashed lines denote the 90% confidence of the linear fit.

Fig. 4. Distribution of the bias error for the whole cloud water samples (black) and for cloud samples discretized as a function of different iron concentration ranges (in color). The bias error is defined by the ratio ($R^f_{HO^\bullet}$ mod - $R^f_{HO^\bullet}$ exp) / $R^f_{HO^\bullet}$ exp in (%). The number of samples analyzed is indicated above each box plot. The bottom and top lines correspond to the 25th and 75th percentiles, respectively. The full line represents the median values. The ends of the whiskers are the 10th and 90th percentiles.

Fig. 5. Distribution of the bias error for the whole cloud water samples for the reference case and for two sensitivity tests performed with the model: (i) the iron chemistry (photolysis of Fe(III) and the Fenton reaction) is neglected in the model; (ii) the iron chemistry is neglected, and the new photolysis rate constants obtained from experimental measurements are implemented in the model. The bias error is defined by the ratio ($R^f_{HO^\bullet}$ mod - $R^f_{HO^\bullet}$ exp) / $R^f_{HO^\bullet}$ exp in (%).The number of samples analyzed is indicated above each box plot. The

bottom and top lines correspond to the 25th and 75th percentiles, respectively. The full line represents the median values. The ends of the whiskers are the 10th and 90th percentiles.

Fig. 6. Distribution of relative contributions of modeled $HO^{\bullet}$ formations rates for each photochemical source (H_2O_2, NO_3^- and NO_2^- photolysis) for the whole cloud water samples. Model outputs are obtained from the sensitivity test in which the iron chemistry is not considered, and new photolysis rate constants from experimental measurements are implemented in the model. The number of samples analyzed is indicated above each box plot. The bottom and top lines correspond to the 25th and 75th percentiles, respectively. The full line represents the median values. The ends of the whiskers are the 10th and 90th percentiles.

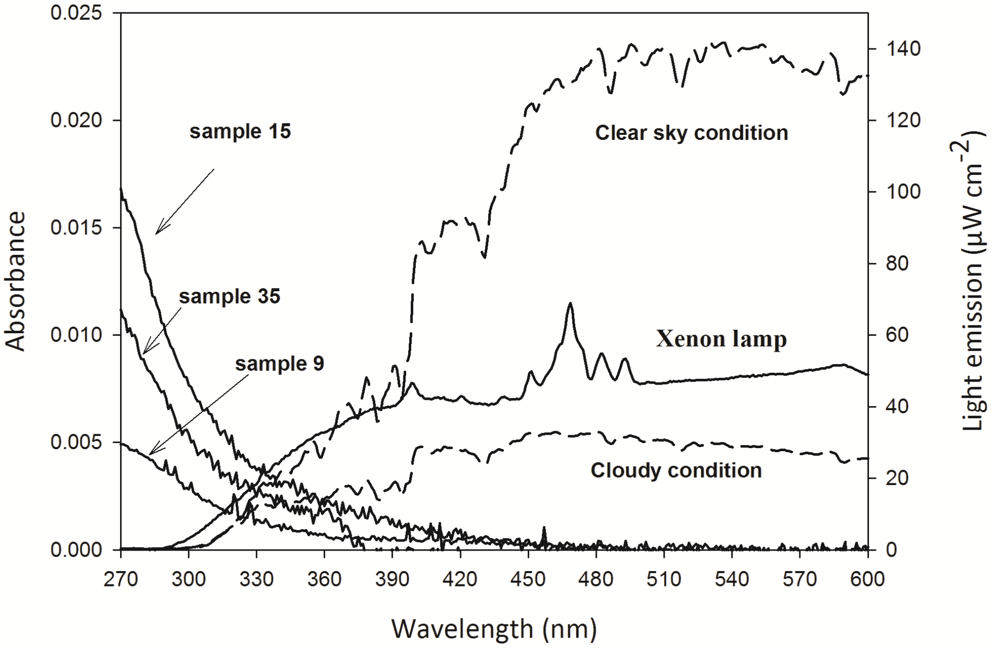

Fig. 1. Absorption spectra of different cloud water samples (left axis) and the right-hand axis shows the emission spectrum of the adopted Xenon lamp reaching solutions over the range of 290 to600 nm (total flux intensity = 157 W m^{-2}) compared with the sun emission spectrum (dashed line) for a sunny (353 W m^{-2}) and a cloudy day (90 W m^{-2}) in October 2013.

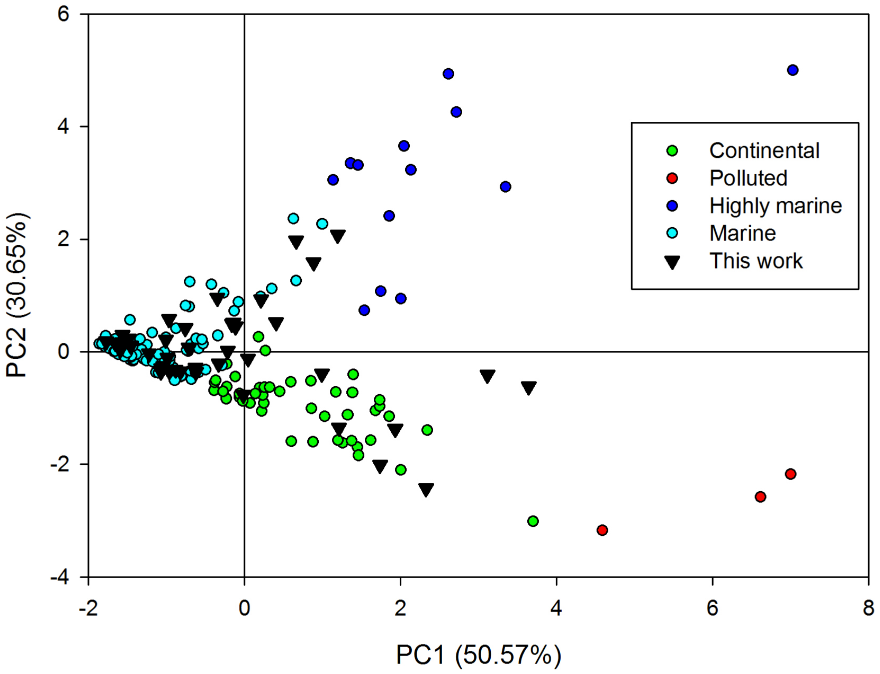

Fig. 2. Scores plot obtained by PCA analysis of 137 samples collected before 2013 and grouped in four classes as a function of the previously described classification (Deguillaume et al., 2014) and 41 samples collected during 2013 and 2014. These new data correspond to 15 cloud events and are indicated in black triangles. Statistical analysis is performed using 6 selected variables (pH, [Na$^+$], [Cl$^-$], [SO$_4^{2-}$], [NO$_3^-$], and [NH$_4^+$]). The scree plot obtained from autoscaled data shows that two selected principal components (PC) containing a total variance of about 81%.

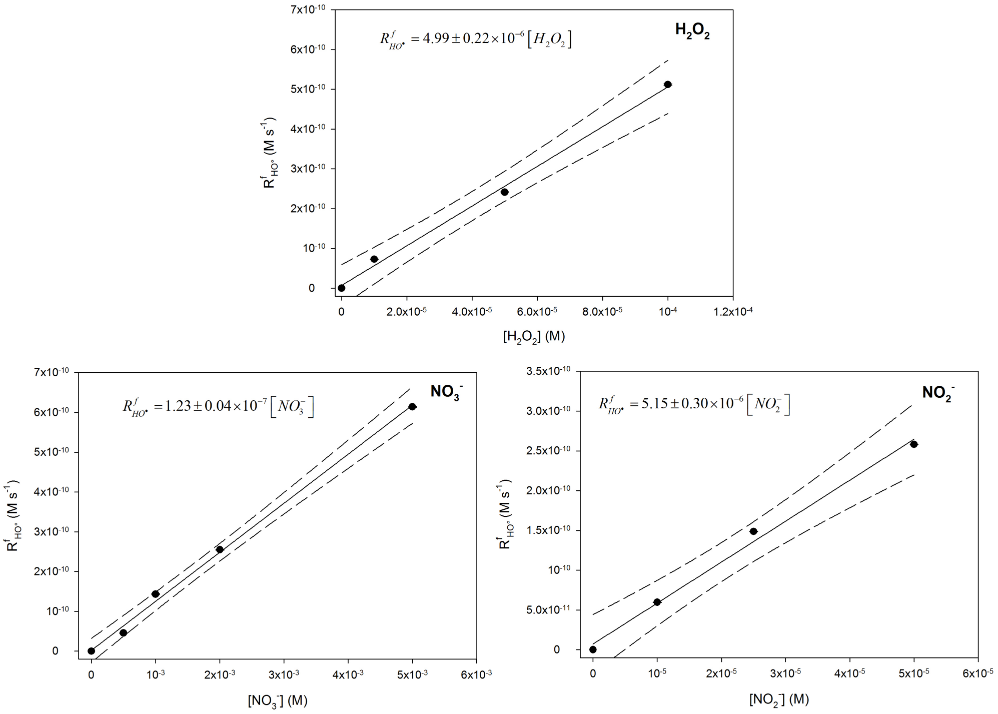

Fig. 3. Scatter plot of hydroxyl radical formation rates *vs*. hydrogen peroxide, nitrate and nitrite concentrations using 2 mM of TA at pH 5.0 under Xenon lamp irradiation. The solid line is the linear fit, and dashed lines denote the 90% confidence of the linear fit.

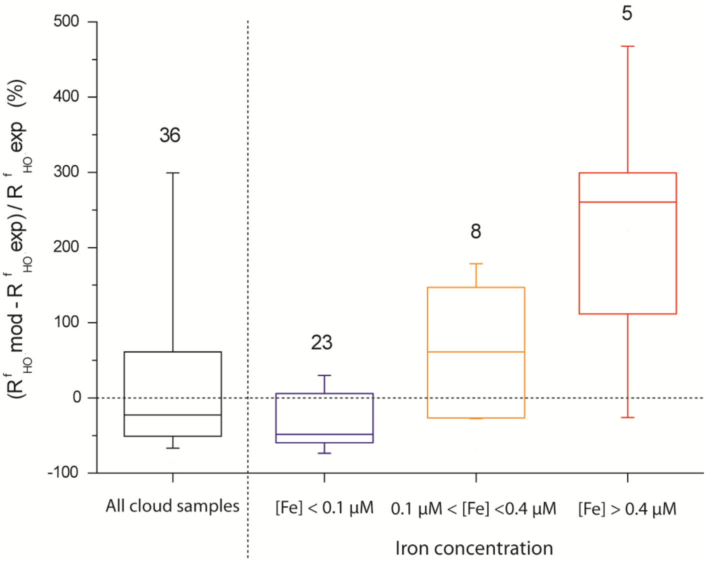

Fig. 4. Distribution of the bias error for the whole cloud water samples (black) and for cloud samples discretized as a function of different iron concentration ranges (in color). The bias error is defined by the ratio ($R^{f}_{HO^\bullet}$ mod - $R^{f}_{HO^\bullet}$ exp) / $R^{f}_{HO^\bullet}$ exp in (%). The number of samples analyzed is indicated above each box plot. The bottom and top lines correspond to the 25th and 75th percentiles, respectively. The full line represents the median values. The ends of the whiskers are the 10th and 90th percentiles.

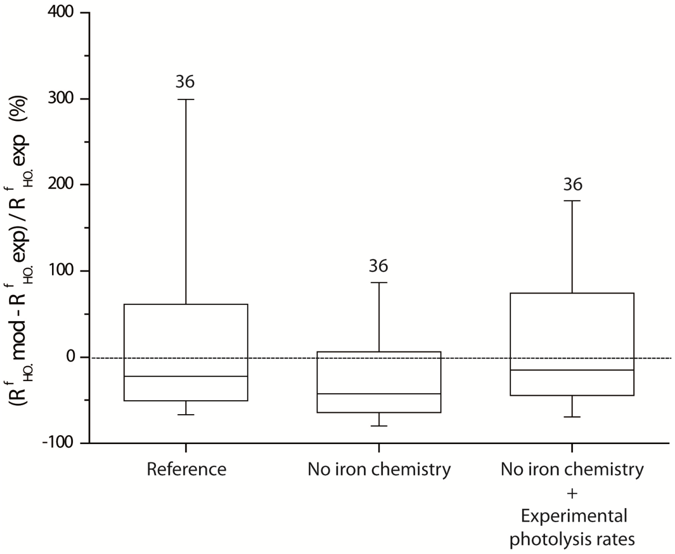

Fig. 5. Distribution of the bias error for the whole cloud water samples for the reference case and for two sensitivity tests performed with the model: (i) the iron chemistry (photolysis of Fe(III) and the Fenton reaction) is neglected in the model; (ii) the iron chemistry is neglected, and the new photolysis rate constants obtained from experimental measurements are implemented in the model. The bias error is defined by the ratio ($R^f_{HO^\cdot}$ mod - $R^f_{HO^\cdot}$ exp) / $R^f_{HO^\cdot}$ exp in (%).The number of samples analyzed is indicated above each box plot. The bottom and top lines correspond to the 25th and 75th percentiles, respectively. The full line represents the median values. The ends of the whiskers are the 10th and 90th percentiles.

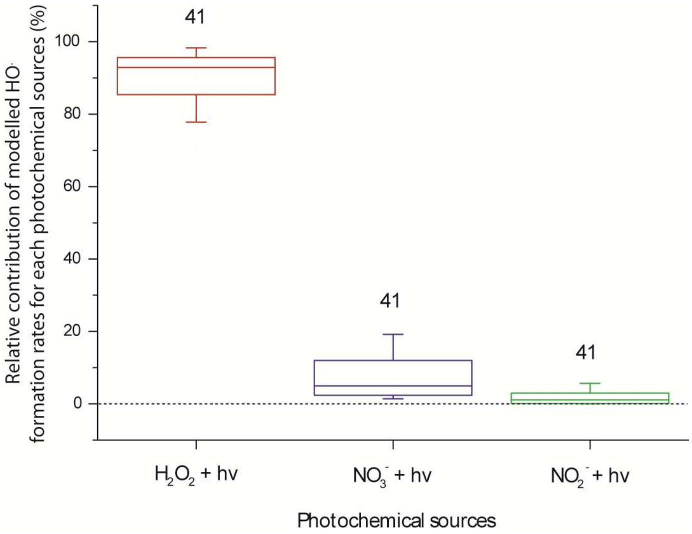

Fig. 6. Distribution of relative contributions of modeled $HO^\bullet$ formations rates for each photochemical source (H_2O_2, NO_3^- and NO_2^- photolysis) for the whole cloud water samples. Model outputs are obtained from the sensitivity test in which the iron chemistry is not considered, and new photolysis rate constants from experimental measurements are implemented in the model. The number of samples analyzed is indicated above each box plot. The bottom and top lines correspond to the 25th and 75th percentiles, respectively. The full line represents the median values. The ends of the whiskers are the 10th and 90th percentiles.